Collagen suprafibrillar confinement drives the activity of acidic calcium-binding polymers on apatite mineralization

Jérémie Silvent, Marc Robin, Camila Bussola Tovani, Yan Wang, Fabrice
Soncin, Sidney Delgado, Thierry Azaïs, Capucine Sassoye, Marie-Madeleine
Giraud-Guille, Jean-Yves Sire, et al.

Bio MACROMOLECULES

Article

Collagen Suprafibrillar Confinement Drives the Activity of Acidic Calcium-Binding Polymers on Apatite Mineralization

Jérémie Silvent, Marc Robin, Camila Bussola Tovani, Yan Wang, Fabrice Soncin, Sidney Delgado, Thierry Azaïs, Capucine Sassoye, Marie-Madeleine Giraud-Guille, Jean-Yves Sire, and Nadine Nassif*

Cite This: https://doi.org/10.1021/acs.biomac.1c00206

Read Online

ACCESS | ili Metrics & More | 🔳 Article Recommendations | SI Supporting Information

ABSTRACT: Bone collagenous extracellular matrix provides a confined environment into which apatite crystals form. This biomineralization process is related to a cascade of events partly controlled by noncollagenous proteins. Although overlooked in bone models, concentration and physical environment influence their activities. Here, we show that collagen suprafibrillar confinement in bone comprising intra- and interfibrillar spaces drives the activity of biomimetic acidic calcium-binding polymers on apatite mineralization. The difference in mineralization between an entrapping dentin matrix protein-1 (DMP1) recombinant peptide (rpDMP1) and the synthetic polyaspartate validates the specificity of the 57-KD fragment of DMP1 in the regulation of mineralization, but strikingly without phosphorylation. We show that all the identified functions of rpDMP1 are dedicated to preclude pathological mineralization. Interestingly, transient apatite phases are only found using a high nonphysiological concentration of additives. The possibility to combine biomimetic concentration of both collagen and additives ensures specific chemical interactions and offers perspectives for understanding the role of bone components in mineralization.
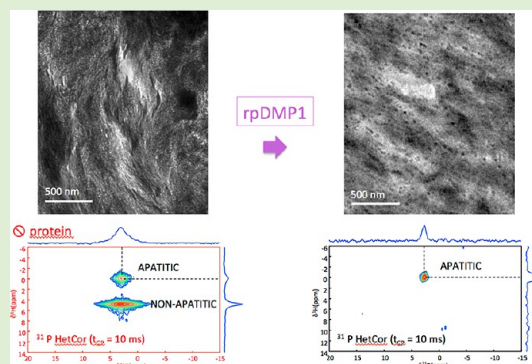
■ INTRODUCTION

Bone is a complex composite material, which closely associates cells and an extracellular matrix (ECM). The bone ECM combines various components, that is, collagen, noncollagenous proteins (NCPs), carbonated hydroxyapatite (HA) nanoparticles, and water. Although bone is one of the most studied living materials, the exact role of its components, noticeably the organic one, is still debated. Both intra-[1−3] (~40 nm) and interfibrillar[4] (~1.5 nm) spaces in collagen are proposed to be nucleation sites for bone mineral. The interfibrillar confinement generated by the collagen matrix increases as the ECM becomes mineralized, thus forming the mature bone (Figure 1A) with the characteristic twisted plywood pattern[5] (Figure 1B). This suprafibrillar three-dimensional (3D) architecture affects the physical properties of the ECM such as mechanical response[6,7] and microenvironment (e.g., size and spatial distribution of apatite, local hydrated environment of phosphate ions).[8] In addition, *in vitro* investigations on NCPs activity have indeed yielded contradictory findings when the protein is studied either in solution or in gel.[9,10] Upon working with gels, loose collagen matrices imply large interfibrillar spaces due to the lack of collagen packing,[8] meaning that bone is only reproduced at the fibril level.[11,12] Consequently, aside *in vivo*-based experiments, biomimetic models in terms of confinement are needed to ensure that investigations of NCPs activity are conducted

under native environment. As demonstration, only models mimicking both collagen density and geometry described for mature bone (250 mg/mL)[8] tissues led to the typical apatite/collagen co-alignment (Figure 1C), but noticeably with higher concentrations of calcium ions (Figure 1D, left) than that described in extracellular fluid (ECF).[13] Indeed, simulated body fluid (SBF) failed to produce intrafibrillar mineral; instead, apatite in the form of spherulite was found (Figure 1D, right). This result suggested that Ca-rich proteins from bone ECM concentrate ions in the gap regions.

To go further on the effect of bone ECM confinement on NCPs activity, we pursue the study by entrapping dentin matrix protein-1 (DMP1), an acidic calcium-binding polymer[14] within our models. DMP1 is a phosphorylated ECM protein produced by osteocytes and odontoblasts that is commonly accepted as mediator in bone mineralization processes.[15−17] Indeed, DMP1 knockout mice display defective mineralization of dentin[18−21] and bone[22,23] resembling phenotypes observed in human genetics. Interestingly, the
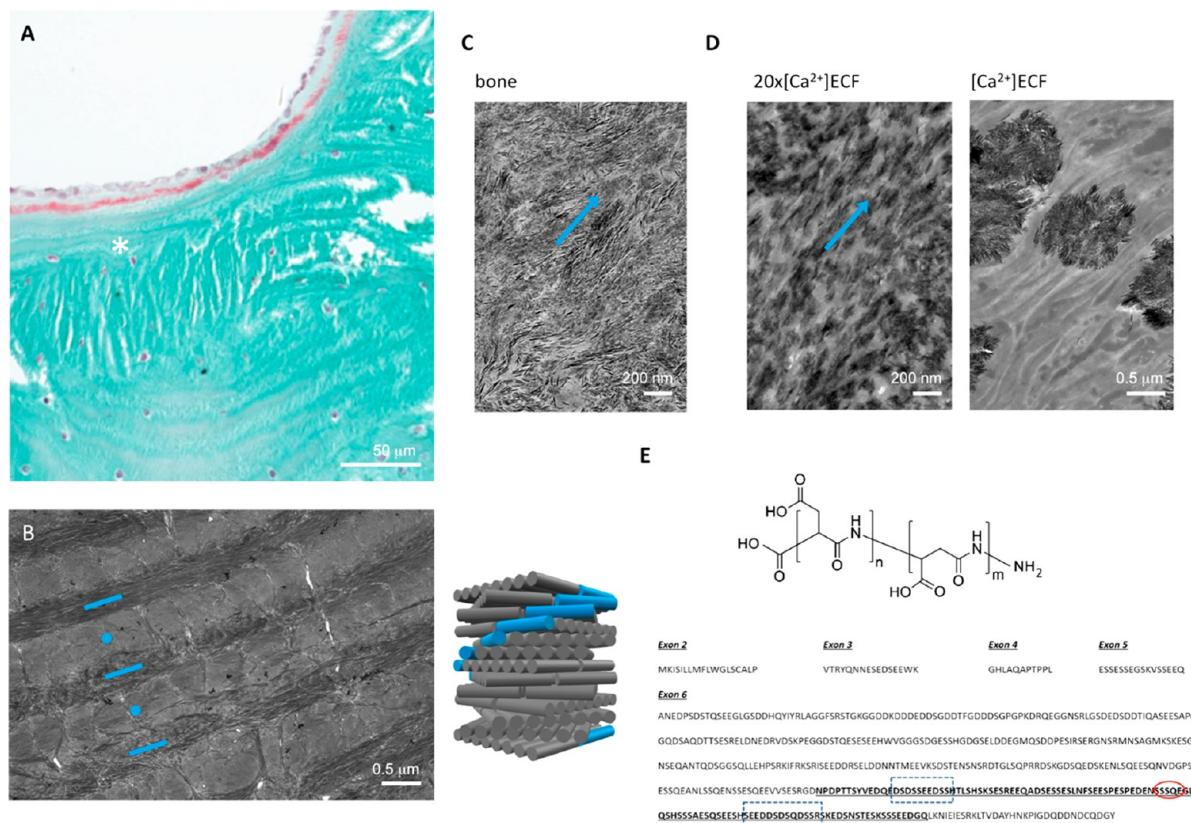
Figure 1. Comparison of collagen/apatite relationship in bone and in synthetic models reproducing the collagen confinement (density and order) found in bone. (A) Thin section of bone stained with Masson's trichrome. From top to bottom: Osteoblasts, osteoid tissue (light blue and red), and mature bone (*). Transmission electron microscopy ultrathin sections of (B) mature decalcified human bone that is characterized by a twisted plywood organization of collagen fibrils (blue dot and bars represent molecules that are perpendicular and parallel to the observation plan, respectively) schematically represented, (C) unstained sheep bone where the alignment of apatite platelets along the fibril is observed (the blue arrow shows the orientation), (D) Coll/CHA/SBF (left) and Coll/SBF/SBF (right) where $[Ca^{2+}] = 20[Ca^{2+}]ECF$ and $[Ca^{2+}] = [Ca^{2+}]ECF$, respectively. The collagen/apatite co-alignment similar to that in bone is observed in Coll/CHA/SBF (left) while spherulitic apatite crystals are obtained in Coll/SBF/SBF (right). In (E), the acidic calcium-polymer used in the biomimetic model, that is, the polyaspartate formula and the human DMP1 sequence (in bold: target peptide; blue boxed texts: collagen binding sites; red encircled text: motif found as unchanged during 220 My). The influence of organic polymers on apatite formation is studied at fixed physiological concentration of calcium, that is, $[Ca^{2+}] = [Ca^{2+}]ECF$ with two different concentrations for rpDMP1 as follows: 2.5 $\mu g/mL$ (1rpDMP1) and 25 $\mu g/mL$ (10rpDMP1).

role of DMP1 has been investigated *in vitro* through different models (e.g., in solution,[24,25] adsorbed onto glass plates,[14,26] in gelatin-gel systems,[15,27] on a transmission electron microscopy (TEM) grid coated with recombinant spider silks,[28] with preassembled collagen fibrils,[29,30] and with early calcifying bone-like matrix),[31] reaching the conclusion that the protein could be involved at different levels including in apatite nucleation control[27,32] and growth inhibition,[33] in mediating the size of collagen fibrils,[29] and in stabilizing amorphous calcium phosphate (ACP) phase.[33,34] To clarify such functional diversity, a DMP1 recombinant peptide (rpDMP1) containing those two collagen binding sites[29] and the peptide [427]SSSQE[431] was synthesized and used here (unphosphorylated, 121 amino acids, 13 kDa, pI = 4.14) (Figure 1E, down). Indeed, four DMP1 peptides are identified in dentin and bone extracts: (1) the full-length protein, (2) a N-ter fragment of 37 kDa, (3) a C-ter fragment of 57 kDa,[35] and (4) a proteoglycan derived from the N-ter fragment and known as DMP1-PG found in rat and mouse.[36] Importantly, five highly conserved motifs during mammalian evolution were identified including [427]SSSQE[431], suggesting the importance of this acidic peptide for the protein structure and/or function.[37] Moreover, it was reported that the 57 kDa fragment recapitulates the function of

full-length DMP1 in regulation of mineralization and osteocyte maturation.[38] Finally, phosphorylation appears to be dedicated to the organization of mineral when there is no collagen fibrillar packing[39] since both phosphorylated and non-phosphorylated rDMP1 are proposed as apatite nucleators.[40]

In addition to the confinement criterion, the concentration of protein closer to physiological conditions[41,42] is of importance to access to their native properties. Noticeably, differences in range of concentrations (factor 10 to 100) can lead to opposite activities[14,15,24,26,29] blurring the conclusions.

To validate the specificity of the 57-KD fragment of DMP1, experiments were also carried out with a synthetic calcium-binding polymer, that is, the biomimetic poly-L-aspartic acid (polyAsp, 1.2 kDa, pI = 2.98) (Figure 1E, up).[43,44] Nowadays, polyAsp is commonly used in biomineralization models for mimicking acidic proteins in biological calcified tissues (nacre, bone, dentin). This polymer is described to allow the intrafibrillar infiltration of both DMP1[45] and apatite ion precursors[46] and consequently the collagen/mineral co-alignment.[47]

Here, we show that collagen suprafibrillar confinement drives the activity of acidic calcium-binding polymers on apatite mineralization. The difference in mineralization between

rpDMP1 and polyAsp illustrates the specificity of NCPs amino acids sequence. Under confinement (i.e., intra- and interfibrillar spaces), we show that all the identified functions of rpDMP1 are dedicated for proper calcification to occur, namely the collagen/apatite co-alignment.[48,49] Indeed, we show that while collagen nucleates apatite, rpDMP1 (i) concentrates the apatite ion precursors locally, interfering as a supporting agent for collagen (ii) to induce the formation of a first highly crystalline apatite crystal. In addition, we discard that rpDMP1 stabilizes the possible transient precursors of bioapatite[50,51] since they only form at high nonphysiological concentrations of protein. Finally, (iii) we confirm that it inhibits the apatite growth, but (iv) also show that it might inhibit the homogeneous nucleation irrespective of confinement. Overall, the work demonstrates that aside from cellular and biochemical processes, physicochemical parameters take part in the control of bone biomineralization.

■ MATERIALS AND METHODS

Synthesis and Purification of the Recombinant DMP1 Peptide. *Cloning.* The coding sequence of our targeted human DMP1 peptide (i.e., amino acids 367−481) was isolated from a human primary osteoblast cDNA (Promocell). It was amplified in a thermal cycler (Mastercycler pro, Eppendorf) by PCR using the oligonucleotides 5′ ATGC CATATG AACCCCGACCCCA 3′ and 5′ GCAT CTCGAGTCA GTG GTG GTG GTG GTG GTG GTG CAACTGGCCATCTTC 3′ to create NdeI and XhoI restriction sites at the start and stop codon, respectively. Cycling conditions were initial denaturation at 94 °C for 2 min, followed by 35 cycles, each cycle consisting of 30 s of denaturation at 94 °C, 45 s of annealing at 60 °C and 45 s of elongation at 72 °C. The final elongation lasted for 2 min at 72 °C. PCR products were analyzed by 1% agarose gel electrophoresis and observed in an analyzer Gel Doc (BIORAD, France) after ethidium bromide staining. The amplified fragment was purified using the QIAquick PCR purification kit (Qiagen SA) and digested with NdeI and XhoI restriction enzymes. The resulting products were separated by a migration in a 1.5% agarose gel with ethidium bromide and cloned into the pET22b vector (Novagen/VWR International S.A.S) which had been beforehand digested similarly. Competent Novablue cells were transformed with the ligation mix and selected by overnight growth on LB agarose plates containing 70 μg/mL ampicillin. Positive clones were checked for the presence of the 0.8 kb fragment by NdeI and XhoI restriction analysis.

Expression. BL21 (DE3) cells transformed with pET-DMP1 were grown on a rotating table (220 rpm) overnight at 37 °C in LB medium with 50 μM ampicilin. When the optical density at 600 nm of the bacterial broth reached 0.6−0.8, the induction was realized with an addition of 1 mM of isopropyl β-D-1-thiogalactopyranoside. After 3 h, the cells were centrifuged at 5000g for 10 min, and the pellets were frozen at −20 °C until purification.

Purification. Pellets were resuspended in 5 mL of buffer A (PBS 1×, 50 mM imidazole, complete inhibitor mix (Roche), lysozyme, DNase) and lyzed by sonication three times. The bacterial extract was loaded on a 5 mL bed-volume HisTrap column using an Akta Purifier 10 (GE-Healthcare). Buffer A was flowed through the column at 1 mL/min until A_{280} of the flow through reached a stable value. A 60 mL linear gradient of 0−100% Buffer B (PBS 1×, 500 mM imidazole, complete inhibitor mix (Roche), lysozyme, DNase) in buffer A was applied, and 1 mL fractions were collected. Aliquots were analyzed by 10% SDS-PAGE and the gels stained with Coomassie blue to determine the quality of purified rpDMP1 (12 kDa, pI = 4.14) (Figure S6).

Sample Preparation. *Collagen Extraction.* A solution of type I collagen at ∼3 mg/mL in 0.5 M acetic acid was prepared as previously described.[52] The collagen was extracted from rat tail tendons. After a washing step with PBS, tendons were solubilized in 0.5 M acetic acid, and the solution was clarified by centrifugation (21,000 rpm, 2 h, 11 °C). The supernatant was selectively precipitated with 0.3 and 0.6 M of NaCl by two centrifugations (21,000 rpm, 3 h, 11 °C then 4400 rpm, 45 min, 11 °C), in order to remove proteins other than type I collagen and collagen, respectively. The pellets were solubilized in 0.5 M acetic acid and dialyzed against 0.1 M acetic acid in order to remove salts from the solution. A final centrifugation was performed (21,000 rpm, 4 h, 11 °C), and the concentration was adjusted to a final stock concentration of ∼3 mg/mL. The final concentration of type I collagen solution was estimated by hydroxyproline titration.[53]

Synthesis of Collagen/Apatite Matrices. The matrices were prepared according to a procedure that combines injection and reverse dialysis processes (patent WO2011151587A2). The mineralization conditions for collagen matrices (concentrations of components) are summarized in Table 1. Collagen samples were disk-shaped

Table 1. Mineralization Conditions for Collagen Matrices[a]

sample designation	end collagen concentration (mg/mL)	acidic polymer (μg/mL)	HA ion precursors in dialysis solution (acetic acid)	additional SBF bath
Coll	250	−	−	−
Coll/SBF	250	−	SBF	−
Coll/SBF/SBF	250	−	SBF	+
Coll/CHA/SBF	250	−	CHA	+
Coll/SBF(rpDMP1)	250	2.5	SBF	−
Coll/SBF(rpDMP1)/SBF	250	2.5	SBF	+
Coll/10rpDMP1	250	25	−	−
Coll/SBF(10rpDMP1)	250	25	SBF	−
Coll/SBF(10rpDMP1)/SBF	250	25	SBF	+
Coll/SBF(polyAsp)	250	5.75	SBF	−
Coll/SBF(polyAsp)/SBF	250	5.75	SBF	+
CollOsteoid/SBF/SBF	40	−	SBF	+
CollOsteoid/SBF(10rpDMP1)/SBF	40	25	SBF	+

[a]Ionic composition of SBF and CHA solutions are detailed in Table S1.

with a thickness of ∼1 mm and a diameter of ∼10 mm. A soluble acidic collagen solution (1 mg/mL, 0.5 M acetic acid) supplemented by a 1× SBF solution mimicking the ionic compounds found in the human plasma was prepared by diluting the stock solution (3 mg/mL, 0.5 M acetic acid) with a 1.5× SBF acidic solution (0.5 M acetic acid). SBF was prepared as previously described.[54] The concentrations of the salts precursors are summarized in Table S1. Two concentrations of rpDMP1 were added to this solution: 2.5 μg/mL (low) and 25 μg/mL (high) to form the matrices referred as Coll/SBF-rpDMP1 and Coll/SBF-10rpDMP1, respectively. The rpDMP1 control matrix with the highest concentration of rpDMP1 and without mineral (Coll/10rpDMP1) was obtained by diluting the stock solution with acetic acid (0.5 M). Two matrices used as control were prepared: (i) without any organo-mineral additives (Coll) and (ii) with apatite ion precursors but without addition of any acidic polymer (Coll/SBF). The matrices supplemented by polyaspartate (Coll/SBF-polyAsp) were obtained in a similar way, by adding this acidic polymer (5.75 μg/mL, Lanxess-Bayer, BaypureDS100, 1200 g/mol, pI = 2.98) to the acidic collagen solution. To mimic the osteoid tissue[55] CollOsteoid/SBF/SBF, 40 mg/mL collagen matrices were also formed. In this case, 25 μg/mL rpDMP1 was added to the acidic collagen solution forming the matrix referred as CollOsteoid/SBF-10rpDMP1/SBF. All these solutions were continually injected in a closed dialysis chamber for 1 week. The bottom of the chamber contained a dialysis membrane with a molecular weight cut off of 1 kDa. The reverse dialysis process[56] was set against polyethylene glycol (PEG, 35 kDa, Fluka) to
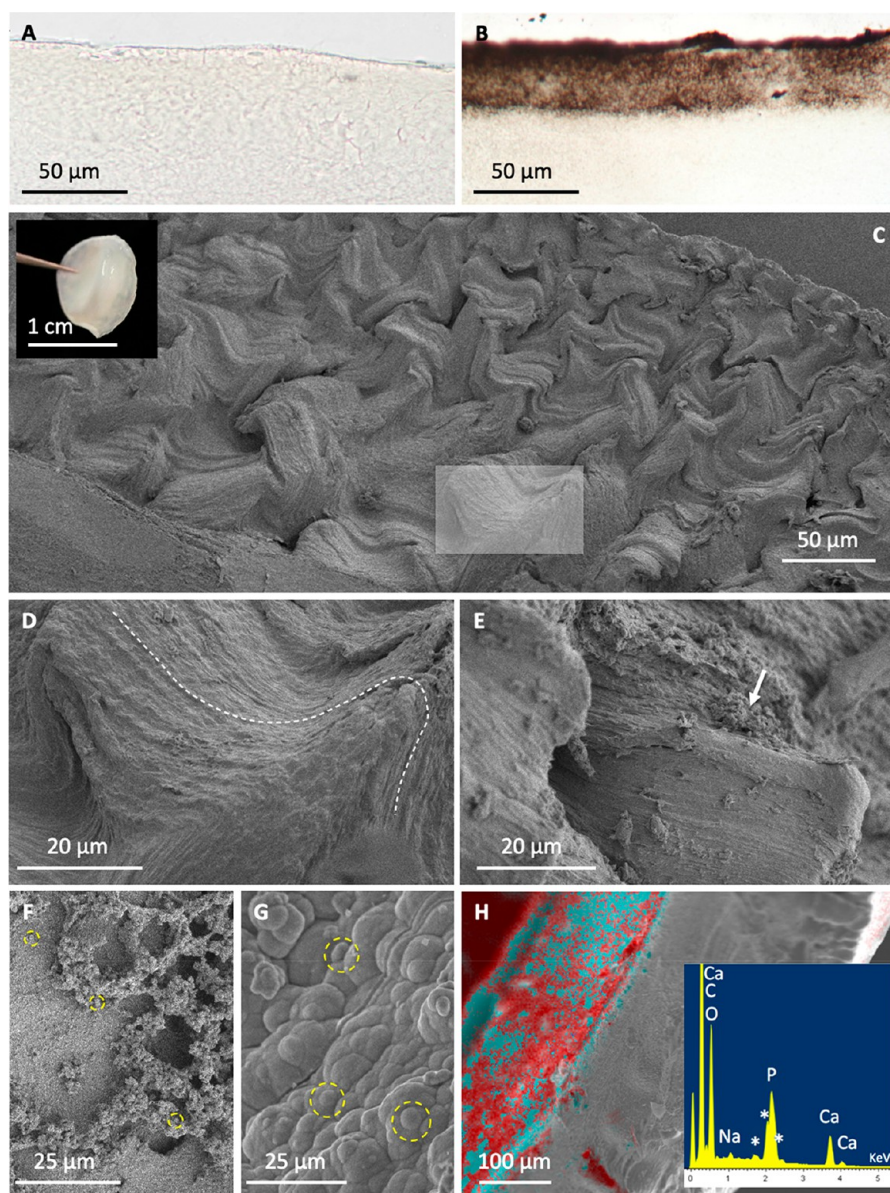
Figure 2. Structural characterizations of the hybrid collagen/apatite matrices in the presence of rpDMP1 containing the highly conserved motif. Histological sections of Coll/SBF(1rpDMP1) (A) and Coll/SBF(1rpDMP1)/SBF (B) stained with von Kossa. SEM observations of the dense collagen matrix (250 mg/mL) at low rpDMP1 content (C−F). Examination of the fractured interior of the disk-shaped matrix (C, inset) before SBF bath (Coll/SBF(1rpDMP1)) (C, D; rectangle in C indicates the enlarged section that is shown in D). Examination after SBF bath (Coll/SBF(1rpDMP1)/SBF): interior (E) and surface (F). In (E), the roughness appears to increase after SBF (arrow). (G) Surface of the collagen matrix precipitated without rpDMP1 (Coll/SBF/SBF). The size and the amount of spherulitic crystals (yellow dashed circles) at the surface of the matrices decrease with rpDMP1. (H) Analysis of Coll/SBF(1rpDMP1)/SBF by EDX coupled with SEM; calcium ions are in red, and phosphorus ions in blue (SEM gold coating*).

control the final concentration of collagen. The PEG was dissolved in 0.5 M acetic acid up to ∼300 mg/mL for all Coll matrices or ∼50 mg/mL for all CollOsteoid matrices. To form the mineralized matrices, the ionic precursors of SBF or CHA were dissolved in the PEG/acetic acid solution. After injection of the total amount of collagen, dialysis was continued for 1 week in order to obtain a homogeneous concentration in the samples and a good maturation of the peptides. The pH was then increased to a range of 9−10 by ammonia gas diffusion for 3 days to induce collagen fibrillogenesis, stabilize the liquid crystalline organization into dense fibrillar matrices, and precipitate the mineral phase. These matrices were then removed from the dialysis chamber and washed several times in sterile double-distilled water until complete neutralization. The final concentration of type I collagen in the different collagen matrices was assessed by hydroxyproline titration and found to be ∼250 mg/mL

for all Coll matrices and ∼40 mg/mL for all CollOsteoid matrices. The different matrices were split into halves, and the mineralization degree of one-half was increased by a bath in 45 mL of 1.5× SBF solution at pH = 7.4 under mild rotary stirring (220 rpm) at 37 °C for 1 week.[8]

Mineral Characterization. *Histology.* Bone samples were fixed in 4% paraformaldehyde and embedded in paraffin for sectioning. Ten μm-thick serial sections perpendicular to the cell layer were dewaxed, rehydrated, and stained specifically by von Kossa, thus identifying divalent ions. The slides were rinsed, dehydrated, and mounted for observation with an optical microscope (Nikon E600 POL) or an epifluorescence microscope (AXIO 100 Zeiss).

Scanning Electron Microscopy and Energy-Dispersive X-ray Spectroscopy. Each sample was fixed in 3.6% glutaraldehyde in a cacodylate/saccharose buffer solution (0.05 M/0.6 M -pH 7.4). The
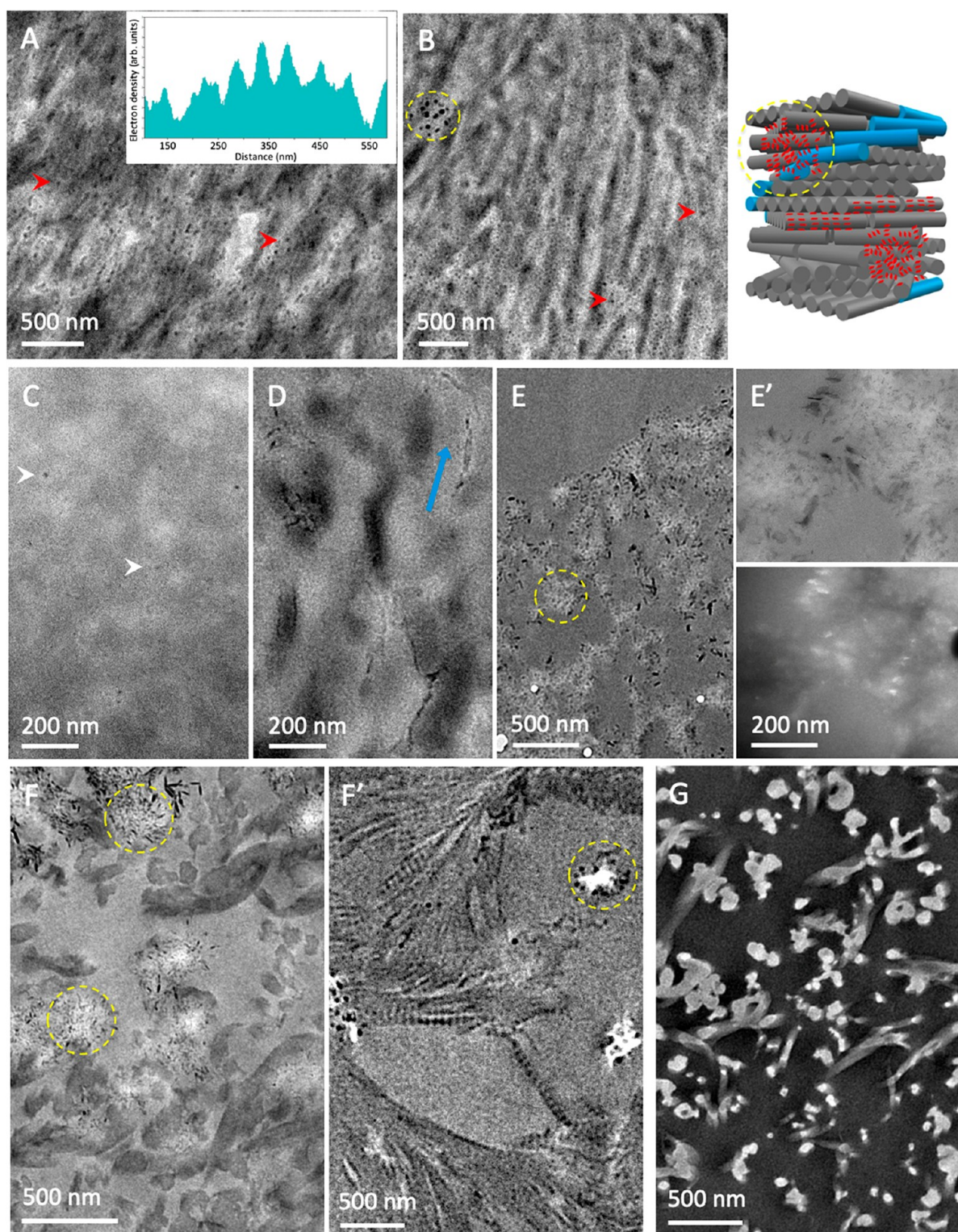
Figure 3. Investigations by TEM of calcium phosphate precipitation in rpDMP1 containing a mature bone-like matrix. Observations of unstained ultrathin sections of (A) Coll/SBF(1rpDMP1) and (B) Coll/SBF(10rpDMP1) before the SBF bath. Both matrices present nanometric electron-dense precipitates (red arrows) along and/or within the collagen fibrils with periodicity highlighted by the intensity profile. In addition, aggregates of the "dot-like" precipitates are seen in Coll/SBF(10rpDMP1); the scheme illustrates the corresponding distribution of dot-like precipitates (red) related to the organization of collagen fibrils. They are found along the fibrils or as aggregates (yellow dashed circle). (C) A control matrix prepared with the high concentration of rpDMP1 (25 μg/mL) and without ionic apatite precursors (Coll/10rpDMP1) shows that collagen fibrils are hardly observed in contrast to the precipitated proteins (yellow arrows). After immersion in SBF, (D) axial alignment of platelets are observed inside the matrix. (E) Observations within the most superficial layer of the matrix show the presence of spherulitic crystals (E′) according to bright-/dark-field images. Observations at the surface of Coll/SBF(10rpDMP1)/SBF (F) without and (F′) with staining where the dashed yellow circles highlight the presence of spherulite. Observations at the surface of (G) Coll without staining.

248 samples were dehydrated through successive ethanol bath (50%, 70%, 249 80%, 90%, and 100%), and a supercritical CO_2 drying process was 250 performed on a BAL-TEC 030. Then samples were sputter-coated 251 with a gold layer of 10 nm and observed in a Hitachi S-3400N 252 operating at 3 kV.

253   Energy-dispersive X-ray (EDX) microanalysis was used for the 254 mapping of mineral deposits inside the matrices. The EDX instrument 255 X-Max (Oxford Instruments) was coupled to a scanning electron 256 microscope Hitachi S-3400N operating at 12 kV, and the Oxford 257 Microanalysis Group XAN.70 software was used for this analysis.

258   *Transmission electron microscopy.* This protocol is similar to the 259 protocol for the scanning electron microscopy (SEM). Then, samples 260 were rinsed, dehydrated, and embedded in Epon 812. For a few 261 samples (always mentioned in the text), an additional postfixation was 262 carried in 2% osmium tetroxide in a cacodylate/saccharose buffer 263 solution (0.4 M/0.6 M-pH 7.4) during 1 h at 4 °C, otherwise neither 264 osmium nor uranyl acetate (staining) were added to avoid artifacts on 265 ultrathin sections. Sections (~80 nm) were observed with a Tecnai 266 spirit G2 operating at 120 kV.

267   *Wide-Angle X-ray Diffraction (Transmission Mode).* Matrices 268 were inserted in X-ray cylindrical borosilicate capillary tubes. The 269 tubes were wax-sealed to keep the samples hydrated and placed 270 directly in the vacuum chamber beam. X-ray diffraction experiments 271 were performed with a S-MAX 3000 RIGAKU using a mono- 272 chromatic CuKα radiation. The diameter of the cylindrical beam 273 dimension of the specimen was 400 μm. The data were collected in 274 the 3−60° range (2θ). The sample-to-detection distance was 0.059 m 275 with a diameter of capillary tubes at 1 mm or 0.058 m with a diameter 276 of 2 mm. The two-dimensional (2D) wide-angle X-ray diffraction 277 (WAXD) patterns were collected with imaging plates then scanned. 278 The data were analyzed using Image (LPS, U-psud) software.

279   *ζ-Potential Measurements.* The matrices were washed before 280 characterization precluding the involvement of free ions in the 281 resulting global charge. Samples were crushed in liquid nitrogen, and 282 the resulting powders were dispersed in PBS solution. Measurements 283 were carried out using a Malvern Zetasizer Nano ZS90.

284   *Thermogravimetric Analysis.* Samples were dried under a laminar 285 hood overnight to minimize the mass loss of loosely bounded water. 286 The analysis was performed on a thermo-microbalance instrument 287 (NETZSCH STA 409PC). The measurement was performed from 288 room temperature to 1000 °C in an oxidizing atmosphere (air) with a 289 heating rate of 5 °C/min.

290   *Nuclear Magnetic Resonance.* Solid-state nuclear magnetic 291 resonance (ssNMR) experiments were realized on hydrated samples. 292 Magic angle spinning (MAS) spectra were acquired at a frequency of 293 8 kHz, with samples packed into 4 mm zirconia rotors. $^1H-^{31}P$ cross- 294 polarization (CP) experiments were performed on an Avance 300 295 Bruker spectrometer operating at frequencies of 300.13 MHz (^1H) 296 and 121.50 MHz (^{31}P). The contact times (CT) were set at 10 and 1 297 ms, and the recycle delay (RD) at 2 s. A 2D $^1H-^{31}P$ heteronuclear 298 correlation (HETCOR) was performed with the following parame- 299 ters: RD = 2 s, CT = 10 and 1 ms, 1280 transients for each 128 t1 300 increments. ^1H and ^{31}P chemical shifts were referenced (δ = 0 ppm) 301 to adamantane and to 85%w aqueous H_3PO_4, respectively.

■ RESULTS AND DISCUSSION

303   **Structural Characterizations of rpDMP1-Loaded Min-** 304 **eralized Collagen Matrices.** Experimental conditions and 305 matrices composition (see Materials and Methods) are 306 summarized in Table 1. It includes collagen matrices without 307 additives used as control, namely Coll, Coll/SBF (Figure S1), 308 Coll/CHA/SBF (Figure 1D, left), and Coll/SBF/SBF (Figure 309 1D, right).[8] This means that after coprecipitation of collagen 310 with either CHA (~20 times more concentrated in apatite ion 311 precursors see Table S1) or SBF, these two last matrices were 312 then immersed in SBF to mimic further steps of mineral 313 growth. With additives (rpDMP1, polyAsp), fibril precipitation 314 was only performed in SBF ($[Ca^{2+}] = [Ca^{2+}]ECF$)[57] to set

315 physiological-like conditions. Two concentrations of rpDMP1 316 were used here, for which we will refer to low (2.5 μg/mL, 317 1rpDMP1) and high (25 μg/mL, 10rpDMP1). For a better 318 reading, data for 10rpDMP1 are displayed in the main text 319 only when differences in mineral formation are observed 320 between the two concentrations. Additional data for 321 10rpDMP1 are shown in Figure S2.

322   We first investigated the spreading of mineral within 323 collagen matrices before and after immersion in SBF for 324 both rpDMP1 concentrations. For this purpose, we used von 325 Kossa staining on histological sections as it allows observations 326 at large scale. Interestingly, staining is hardly observed without 327 SBF extra-bath (Coll/SBF(1rpDMP1), Figure 2A), whereas a 328 strong staining is observed for both matrices at the superficial 329 layer (~50 μm thick) after immersion (Coll/SBF(1rpDMP1)/ 330 SBF, Figure 2B). Because von Kossa staining may interfere 331 with any divalent ions,[58] further characterizations were 332 performed to confirm the presence of mineral.

333   To identify the distribution of the minerals at a lower scale, 334 investigations were performed at the surface and inside 335 fractured disk-shaped matrices (Figure 2C−G) using SEM 336 coupled with EDX microanalysis (Figure 2H). Observations 337 inside the matrix reveal that the entrapment of rpDMP1 does 338 not disturb the self-assembly of collagen fibrils since twisted 339 plywood structures form over large distances (Figure 2C,D 340 versus Figure S1, Coll/SBF). After immersion in SBF (Coll/ 341 SBF(1rpDMP1)/SBF), the surface roughness is more 342 pronounced by the deposition of particles on the closely 343 packed oriented fibrils (Figure 2D versus 2E, arrow). On the 344 surface of the matrices, spherulites usually consisting of 345 aggregates crystals[59] are observed, and, interestingly, they 346 appear to be smaller in the presence of the protein (~0.5 μm 347 versus ~4 μm in Coll/SBF/SBF, yellow dashed circles in 348 Figure 2F,G). In addition, they appear less abundant since they 349 do not cover the whole surface. EDX analysis shows that the 350 spherulites are mainly composed of calcium and phosphorus 351 atoms with an average Ca/P ratio of about 1.66−1.71, 352 suggesting the formation of apatite in the presence of 353 rpDMP1 (Figure 2H).[60]

354   **Confinement Effect on Apatite/rpDMP1 Distribution.** 355 TEM investigations were performed on thin sections of Coll/ 356 SBF(1rpDMP1) and Coll/SBF(10rpDMP1) to access higher 357 magnifications. TEM sections were not stained to avoid the 358 presence of staining deposits that are difficult to distinguish 359 from CaP crystals.[8] Observations evidence the presence of 360 nanometric electron-dense ("dot-like") precipitates (~30 nm) 361 with low and high rpDMP1 concentrations (red arrows in 362 Figure 3A,B, respectively) within the dense collagen network at 363 this scale. The striated pattern (67 nm) is observed locally 364 (Figure 3A, inset), indicating that some minerals localize inside 365 the gap regions.[8,61] Interestingly, additional aggregates of 366 nanoprecipitates are observed for high rpDMP1 content 367 (Figure 3B, yellow dashed circle).

368   To help identify the nature of the "dot-like" precipitates, a 369 control matrix was prepared without apatite ion precursors 370 (Coll/10rpDMP1) (Figure 3C). Likewise, "dot-like" particles 371 are observed (white arrows), confirming that the nano- 372 precipitates are also composed of the protein, in agreement 373 with previous observations.[14] Although it is difficult to 374 conclude due to the low contrast of organic components in 375 TEM, the precipitates appear less abundant and not distributed 376 along the fibrils (Figure 3C versus Figure 3A,B). Nevertheless, 377 spherulites are observed without rpDMP1 in SBF (Coll/SBF/
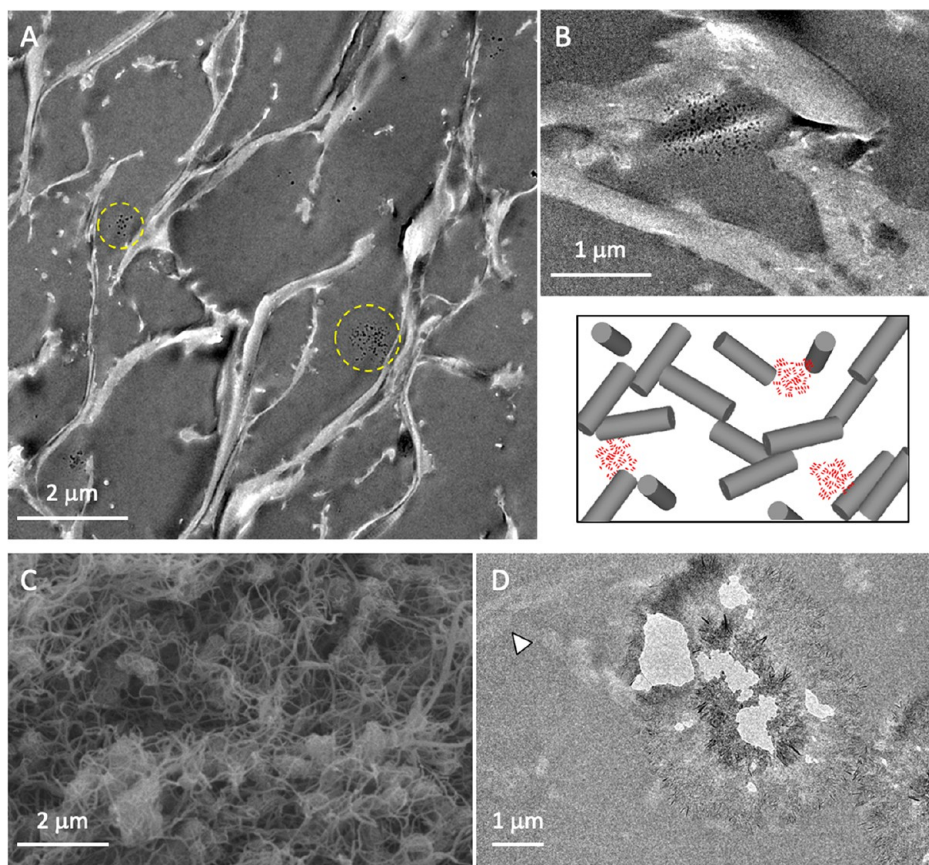
Figure 4. Investigations of calcium phosphate precipitation in rpDMP1 containing osteoid-like matrix. TEM observations of unstained ultrathin sections of CollOsteoid/SBF(10rpDMP1)/SBF (A) at low magnification where "dot-like" precipitates aggregate locally (yellow dashed circle). They are clearly seen (B) at higher magnification. Below, the corresponding relationship between mineral and collagen is represented in the scheme. (C) SEM and (D) TEM micrographs of CollOsteoid/SBF/SBF. The absence of staining makes the observation of cross-striated fibrils usually seen in a longitudinal cut (white arrow) difficult.

378 SBF in Figure 1D and Coll/SBF[8]), indicating that rpDMP1
379 may interfere with some ions to localize specifically inside the
380 gap zone.
381   After a SBF bath, few platelets with axial alignment (blue
382 arrow in Figure 3D) are observed for both rpDMP1
383 concentrations together with spherulitic particles at the surface
384 and within the most superficial layer of the matrix (dashed
385 yellow circles in Figure 3E,F). Noticeably, they appear smaller
386 in size ($\sim$300 nm versus $\sim$2 μm) than those found without
387 rpDMP1 (Figure 1D, right), but remain crystalline according
388 to the contrast observed in the dark-field TEM image (Figure
389 3E′). Further observations at the surface of Coll/SBF-
390 (10rpDMP1)/SBF allow the visualization of both the resin
391 and individual fibril due to a lower density of collagen locally.
392 A comparison between mineralized collagen fibrils without or
393 with staining (Figure 3F,F′, respectively) confirms the
394 precipitation of fibrils with the cross-striated pattern.
395 Observations of an unmineralized collagen matrix without
396 staining (Coll, Figure 3H), where the resin is darker than
397 collagen, confirm that the contrast in mineralized samples
398 comes from the spreading of mineral (ions or precipitates)
399 over the collagen fibrils. Note that we cannot conclude on the
400 involvement of DMP1 in mediating the size of fibrils,[29] since
401 the average diameter of collagen fibrils appears unmodified
402 ($\sim$100 nm) regardless the rpDMP1 concentration.
403   Going further, thermogravimetric analysis (TGA) inves-
404 tigations were performed to better characterize the effect of

405 rpDMP1 concentration on apatite formation (Figure S3).
406 Considering the standard deviation recorded for the matrices
407 ($\pm$5 °C), the difference in mineralization degree should be
408 considered as a trend here. After SBF bath, the mineral content
409 increases for low rpDM1 concentrations (from $\sim$3.5% to
410 $\sim$18%), whereas it does not change significantly at a high
411 content of rpDMP1 (from $\sim$12.5% to $\sim$15%). Since both
412 matrices exhibit spherulites on the surface after SBF bath
413 (Figure 2F and Figure S2C), it indicates that the main mineral
414 content is localized inside the matrix in the form of
415 nanoprecipitates.
416   In addition, the ζ-potential was investigated to help
417 understand the interactions between collagen, rpDMP1, and
418 the mineral. Before the SBF bath, the global surface charge
419 tends to be neutral in the presence of rpDMP1 whatever the
420 concentration of the protein ($-$0.79 ($\pm$0.66) mV and 0.22
421 ($\pm$0.78) mV) for low and high rpDMP1 concentrations,
422 respectively). Indeed, the Coll/SBF matrix exhibits a negative
423 ζ-potential ($-$4.3 ($\pm$2.5) mV.[8] This result agrees with a partial
424 coating of collagen by the selected DMP1 domain, which
425 includes the two collagen binding sites[29] and the highly
426 conserved acidic peptide.[37] Indeed, it is reported that DMP1
427 binds to the N-telopeptide region in collagen.[29,45] After
428 immersion in SBF, Coll/SBF(1rpDMP1)/SBF exhibits a more
429 negative ζ-potential ($-$9.77 ($\pm$0.48) mV)), while it is slightly
430 unchanged for Coll/SBF(10rpDMP1)/SBF ($-$1.79 ($\pm$0.33)
431 mV). The ζ-potential of HA being negative between pH 5 and

pubs.acs.org/Biomac

8 (−5 to −37 mV respectively)[62] is in agreement with the TGA analysis.

To go deeper in the understanding of how the suprafibrillar confinement affects the spreading of rpDMP1 over collagen, the peptide was entrapped in a scaffold mimicking the fibrillar arrangement of osteoid tissue (Figure 4A,B). As mentioned above, this means that (i) the fibrils network is not as dense as the previous mature bone model with larger interfibrillar spaces which are above the micron size (macroporous gel) and (ii) the collagen fibrils are not organized (no plywood geometry). Note that spherulitic crystals form in the control matrix without peptide (CollOsteoid/SBF/SBF) as shown by SEM (Figure 4C) and TEM (Figure 4D), which is in agreement with previous observations on a matrix with a collagen gradient concentration.[8]

Interestingly, "dot-like" precipitates are also observed, but they do not localize inside the fibrils (Figure 4A). Although most of the investigations have focused on electrostatic interactions to explain the intrafibrillar infiltration of both mineral and proteins in collagen, this difference in apatite crystals distribution in osteoid- and mature bone-like matrices evidence that the suprafibrillar confinement provided by the collagen assembly in bone tissue (i.e., cholesteric geometry) plays a key role on this phenomenon. Thus, it may explain the need of other proteins to infiltrate collagen in models lacking biomimetic interfibrillar spaces (<1.7 nm).[45] The fact that collagen here is continuously in contact with ions (even before mineralization) as occurring in bone strengthens the need of a balance between osmotic equilibrium and electroneutrality for intrafibrillar mineralization.[63] In addition, the use of biomimetic collagen interfibrillar spaces (in both osteoid- and mature-like matrices) contradicts that rpDMP1 favors the templating of crystal growth.[14] Conversely, according to (i) TEM and SEM investigations where it is observed that the size of spherulites consist of either "dot-like" aggregate or "mature" apatite platelets with (Figures 2F, 3B, and 4A,B) or without rpDMP1 (Figures 2G and 4C,D) respectively, (ii) the mineral amount found by TGA, and (iii) the resulting surface charge probed by ζ-potential, we confirm its role as a growth inhibitor.[33] This effect may be related to the confinement which promotes the protein folding by destabilizing the unfolded state[64,65] and thus further specific interactions between rpDMP1 and apatite nuclei; the structural characteristics of growing apatite being driven by the involvement of ionic substitutions (specifically from carbonate ions).[66]

Toward Evidence of the Specific Activity of rpDMP1 under Confinement. When polyAsp is supplemented to collagen, it is difficult to observe a difference in mineral spreading over the collagen matrix before immersion in SBF (Coll/SBF(polyAsp), Figure 5A) as compared to rpDMP1. Here also, a lower concentration of polyAsp (5.75 μg/mL) was used than that in the literature (usually between 10 and 100 μg/mL) (i) to reach at least 2 magnitude order lower amounts of negative charge and (ii) to reproduce a more "realistic" collagen to NCPs ratio since such a high polyAsp concentration can be used for one single fibril.[3] Note that our samples were not lyophilized before characterization, as it is commonly performed with this polymer in the literature.[67] This is of importance since the resulting phase and degree of mineralization are here related to a hydrated biomimetic process. The difference between polyAsp and rpDMP1 in apatite mineralization becomes clearer after the SBF bath (Coll/SBF(polyAsp)/SBF, Figure 5B,C). TEM observations
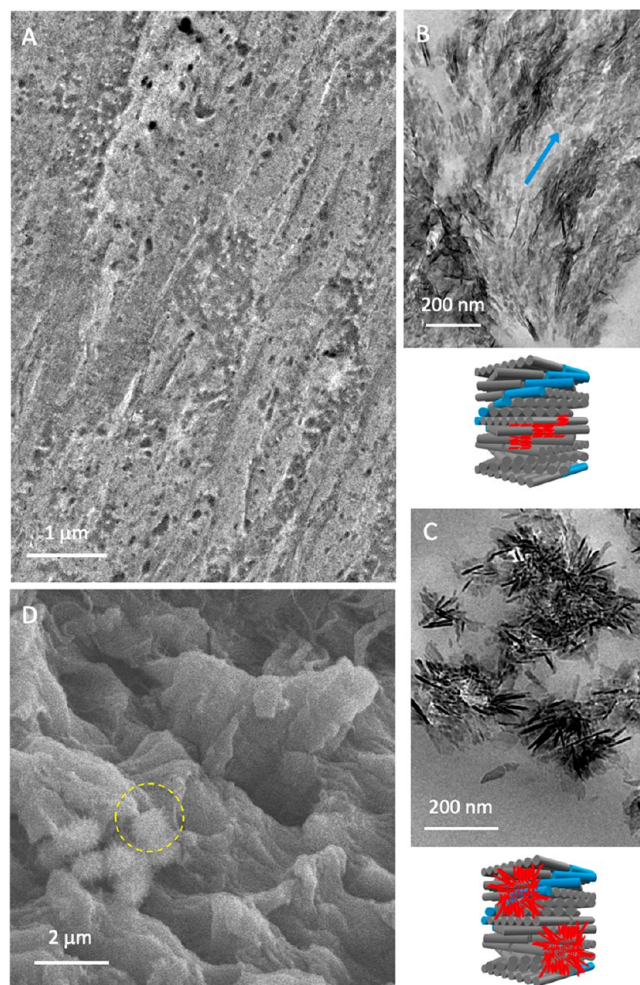

Figure 5. Calcium phosphate precipitation investigated by EM in the presence of polyAsp containing mature bone-like matrix. Observations by TEM of unstained ultrathin sections of matrices before and after SBF immersion: (A) Coll/SBF(polyAsp) and (B,C) Coll/SBF-(polyAsp)/SBF, respectively. The corresponding schematic representation of the apatite crystal (red)/collagen fibril (gray) relationship in a 3D perspective is shown. The lack of staining in (A) indicates that there is an homogeneous spreading of SBF ions over the collagen. After immersion in SBF (B, C), HA platelets are observed in the matrix; they either (B) co-align with the long axis of the fibril (blue arrow) or (C) form spherulites as schematically presented, respectively, below the (B) and (C) TEM micrographs. (D) SEM micrograph of Coll/SBF(polyAsp)/SBF showing that spherulites (yellow dashed circle) are also observed inside the matrix.

reveal large domains where the mineral platelets co-align with the collagen fibrils (Figure 5B), as seen in mature bone (Figure 1C) strengthening the affinity of polyAsp for gap regions in line with previous conclusions in the literature.[44,45,68] However, in contrast to rpDMP1 results, nonbiomimetic spherulitic crystals are also observed in the matrix (Figure 5C,D), strengthening that only small molecules such as osteocalcin can penetrate alone the intrafibrillar space.[69]

These observations evidence the specificity of biological rpDMP1 versus synthetic polyAsp amino-acids sequences in mediating apatite mineralization and also suggest that, in addition to its role as growth inhibitor, it may prevent homogeneous nucleation.[33] Finally, because the rpDMP1 sequence is not phosphorylated, this result tends to strengthen
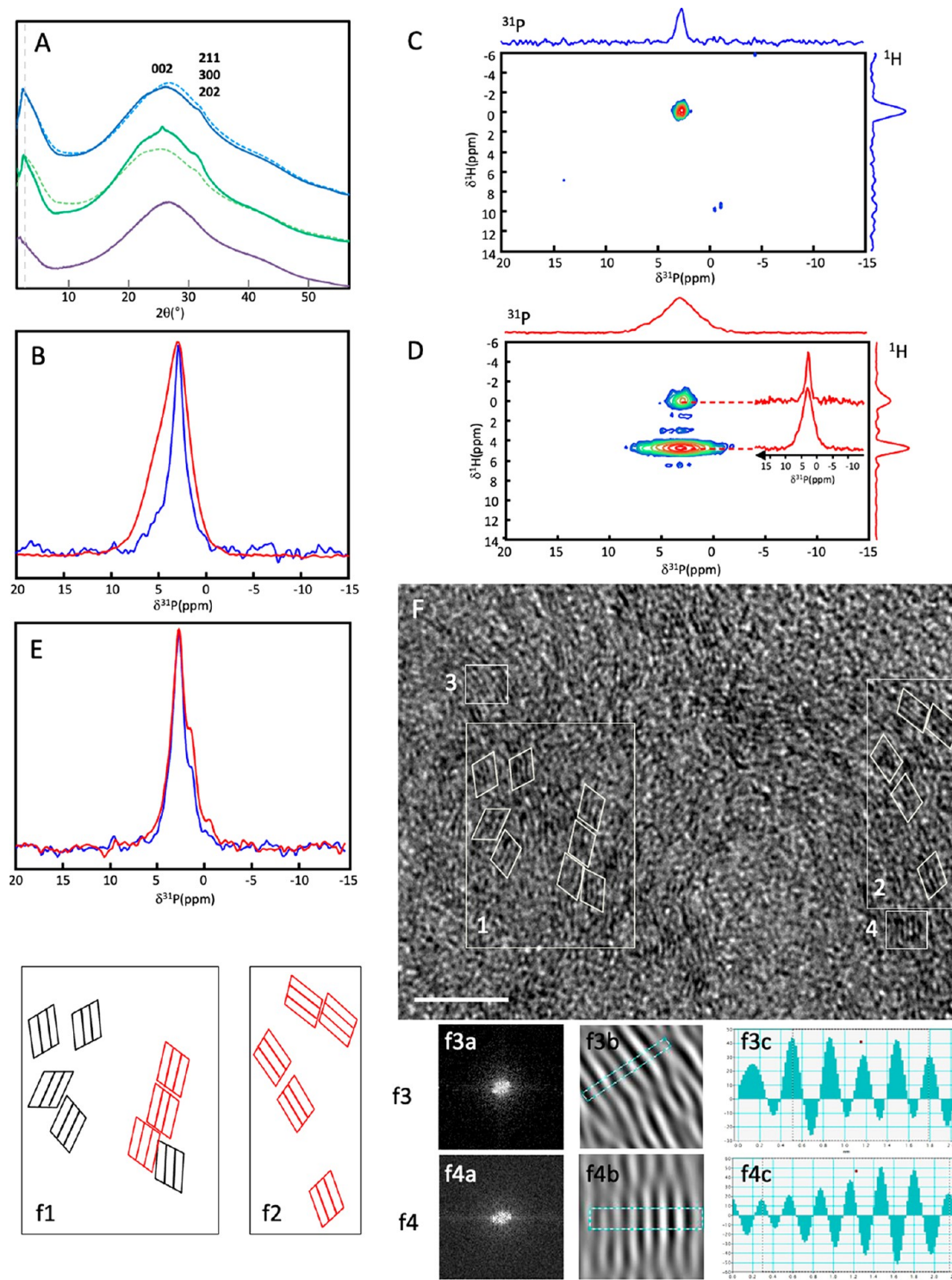
Figure 6. Characterization of the mineral phase. (A) 1D radial average of the WAXD patterns of matrices at 2.5 μg/mL, without (Coll/SBF(1rpDMP1), dashed green) and with (Coll/SBF(1rpDMP1)/SBF, plain green) immersion in SBF; at 25 μg/mL, without (Coll/SBF(10rpDMP1), dashed blue) and with (Coll/SBF(10rpDMP1)/SBF, full blue) immersion in SBF, and a collagen matrix as control (purple). The vertical gray dashed line points out the shift of the reflection which corresponds to the lateral distance between collagen molecules. (B) 1D ^{31}P CP MAS spectra (CT = 10 ms) of the hybrid matrices Coll/SBF(1rpDMP1) (blue) and Coll/SBF(1rpDMP1)/SBF (red). (C) 2D ^{1}H–^{31}P HETCOR spectrum (CT = 10 ms) of Coll/SBF(1rpDMP1) with extracted ^{31}P slices at $\delta(^1$H) = 0 and 4.9 ppm. (D) 2D ^{1}H–^{31}P HETCOR spectrum (CT = 10 ms) of Coll/SBF(1rpDMP1)/SBF. (E) 1D ^{31}P CP MAS spectra (CT = 10 ms) of the hybrid matrices Coll/SBF(10rpDMP1) (blue) and Coll/SBF(10rpDMP1)/SBF (red). (F) TEM micrograph of Coll/SBF(1rpDMP1)/SBF (scale bar = 5 nm) showing crystalline HA nanodomains. (f1) and (f2) are schematic representations of the selected areas 1 and 2 showing the orientation of the HA (210) planes; some crystalline nanodomains appear to align along the same direction (red). (f3) and (f4) FFT (f3a and f4a) and inverse FFT (f3b and f4b) performed on the selected areas 3 and 4, confirming the presence of crystalline nanodomains. The d spacings are measured using the inverse FFT profile along one direction (f3c and f4c).

that the organic phosphate concern may be attributed to polyadenosine diphosphate ribose.[70]

Structural Features of rpDMP1-Mediated Mineral under Confinement. WAXD studies were performed to better characterize the mineral phase and collagen network. The 1D radial average of the WAXD patterns is shown in Figure 6A. Without the SBF extra bath, the signal from collagen fibrils is strong, revealing a low degree of mineralization (dashed green and blue lines). The characteristic HA diffraction peaks, that is, (002) and the merged (211), (300), (202) reflections, are observed more clearly after the SBF bath (full green and blue lines), especially for Coll/SBF(1rpDMP1)/SBF, confirming an increase in mineral content. In addition, the lateral distance between collagen molecules decreases from 1.5 to 1.1 nm in the matrices loaded with rpDMP1 (with or without SBF bath) in comparison to the pure collagen matrix (full purple line) as observed by the peak shift toward high angles (vertical gray dashed line). This distance is shorter than that reported for a mineralized dense collagen scaffold without protein,[7] but agrees with densely packed microfibrils[71] and fibrillar collagen in a dry state.[72] Since the sample is studied in its native hydrated form, this decrease in the intermolecular distance in addition to the contrast observed in fibrils by TEM confirm that rpDMP1 localizes inside the gap zones. The peptide may colocalize with the mineral as shown for polyelectrolytes.[63] Besides confinement, SBF ions are needed for the protein to localize in intrafibrillar spaces, especially calcium ions, considering the model of a periodic assembly of DMP1 into a β-sheet template with high calcium-binding capacity.[14] Then the Ca-binding protein can interact with a significant fraction of the π, that is, possibly covalently bond to the collagen.[73] At a critical concentration of Ca^{2+}, the apatite nucleation which strongly depends on the degree of confinement[74] that occurs inside collagen. However, since apatite forms without organic additives under collagen confinement,[8] it shows that rpDMP1 increases the local ions concentration but does not initiate the nucleation here.

To investigate the presence of calcium-phosphate minerals described as transient phases in bone formation[51,75,76] and better understand the local phosphate environment in collagen-containing rpDMP1, ^{31}P ssNMR experiments were performed (Figure 6B–E). The ^{31}P CP MAS spectrum of Coll/SBF(1rpDMP1) displays a single ^{31}P resonance centered at 2.8 ppm, typical of apatite (Figure 6B, blue). Interestingly, the 2D $^{1}H-^{31}P$ HETCOR spectrum of Coll/SBF(10rpDMP1) does not show the correlation resonance characteristic from HPO_4^{2-} (Figure 6C), excluding the presence of a hydrated disordered surface layer.[66,77] In addition, the line width of the ^{31}P resonance (LW = 1 ppm) is thinner than matrices prepared without rpDMP1 (Coll/SBF, LW = 2 ppm) (Figure S4). Both the thinner resonance and the absence/low amount of HPO_4^{2-} surface species demonstrate that the mineral "dot-like" precipitates of the matrices are highly crystalline and that rpDMP1 drives the higher crystallinity of apatite. This result is in agreement with previous works proposing that DMP1 impacts on the initial stages of apatite formation, providing a structural local order.[14] Interestingly, DMP1 is found more abundant in the boundary between the dentin and enamel where apatite is well crystallized.[30]

Finally, it is interesting to note that such "dot-like crystals" were found at the very early stages of normal *in vivo* calcification.[1] After the SBF bath, the ^{31}P LW in CP MAS spectrum increases (Figure 6B, red), reaching the value found for bone apatite (4.1 ppm).[78] The fact that the 2D $^{1}H-^{31}P$ HETCOR spectrum of Coll/SBF(1rpDMP1)/SBF (CT = 10 ms) (Figure 6D) displays the two typical resonances of bone minerals, that is, $\delta(^{31}P)$ = 2.8 and 3.2 ppm, shows that the apatite spherulites observed at the surface of the matrices by microscopy (Figure 2F) dominate the spectroscopic signature here.

At a higher rpDMP1 content, 1D ^{31}P CP-MAS spectra (Figure 6E) display two shoulders (centered at 1.5 and −1 ppm) in addition to the apatite resonance at 2.8 ppm before and after SBF. These resonances correspond to the HPO_4^{2-} ions from the OCP phase. Noticeably, the presence of a relatively low content of rpDMP1 leads to the physiological single apatitic phase, whereas a high "nonphysiological" concentration of protein stabilizes an additional CaP phase like OCP. Such high concentrations are classically used in the literature, questioning the role of DMP1 in stabilizing the ACP phase.[33,34]

HRTEM observations performed on ultrathin sections of Coll/SBF(1rpDMP1)/SBF (Figure 6F and Figure S5) confirm the highly crystalline nature of the "dot-like" precipitates. Spaced thin layers that are mostly concentric, that is, onion-like morphology that appears to be composed of crystalline nanodomains (∼1 nm) (some are depicted in areas 1 and 2), are observed. Schematic representations of two selected areas (1 and 2) show the orientation of possible crystal planes (f1 and f2). Some crystalline nanodomains appear to align along the same direction (in red). Their morphology is difficult to identify; they are presented here as parallelogram. In (f3) and (f4), fast-fourier tranform (FFT) (f3a and f4a) and inverse FFT (f3b and f4b) performed on the (3 and 4) selected areas confirm the presence of crystalline nanodomains. The crystal planes were indexed by comparing the measured d spacings using the FFT profile along one direction with calculated values of HA (f3c and f4c). Two lattice spacings were measured as 0.31 and 0.34 nm, corresponding to the known (210) and (002) crystal planes of apatite (Figure 6F and Figure S5, respectively). Among the 20 analyzed planes, 80% correspond to the (210) and the remaining 20% to the (002).

The possible consequence of a crystalline apatite nanodomain versus an ACP phase can prevent the formation of pathological calcifications. Indeed, ACP as the first solid phase of calcium phosphate formed in bone would delay apatite formation, allowing the precipitation of other transient phases. This hypothesis is in agreement with the fact that the mineralization process of bone is described to occur rapidly as soon as collagen molecules self-assemble into collagen fibrils in the extracellular space.[79] In fact, according to our knowledge, there is no report on bone pathologies related to the presence of one of the transient apatite phases, although it is extensively described in synthetic models lacking interfibrillar confinement *in vitro* as discussed above.

■ CONCLUSION

The bone ECM is a dynamic (in terms of structure, remodelling, and ECF) and complex environment where the confinement effect occurs that is not only critical for the cells behavior[80] but also for the proteins and even the solvent (water).[64] Indeed, confinement provided by suprafibrillar organization of collagen strongly impacts the activity of mineralizing polymers. The results suggest the occurrence of

sequential cooperative effects during the early stages of bone apatite precipitation through the formation of Ca-DMP1 complex, which then binds to collagen allowing the concentration of apatite ion precursors in gap regions. Formation of highly apatite nuclei and inhibition of both homogeneous nucleation and crystal growth are consistent with a common role of DMP1 controlling the physiological (versus pathological) bone formation. Strikingly, these effects are reached with the nonphosphorylated 57-KD amino acid sequence under confinement. This versatile bone-like model will be useful to provide insights into the role of other bone components (e.g., citrate, proteoglycans, or even different sequences related to NCPs kinetic of maturation (i.e., post-translation modification)) during the successive events that orchestrate mineralization.

■ ASSOCIATED CONTENT

Ⓢ Supporting Information

The Supporting Information is available free of charge at https://pubs.acs.org/doi/10.1021/acs.biomac.1c00206.

Composition of the solutions used to mineralize collagen matrices, SEM and TEM images, EDX spectra, and TGA curves (PDF)

■ AUTHOR INFORMATION

Corresponding Author

Nadine Nassif − Collège de France, Laboratoire Chimie de la Matière Condensée de Paris, LCMCP, CNRS, Sorbonne Université, F-75005 Paris, France; ⓞ orcid.org/0000-0002-4094-4909; Email: nadine.nassif@sorbonne-universite.fr

Authors

Jérémie Silvent − Collège de France, Laboratoire Chimie de la Matière Condensée de Paris, LCMCP, CNRS, Sorbonne Université, F-75005 Paris, France; MNHN, CNRS, EPHE, Institut Systématique Évolution Biodiversité, ISYEB, Equipe Homologies, Sorbonne Université, 75005 Paris, France

Marc Robin − Collège de France, Laboratoire Chimie de la Matière Condensée de Paris, LCMCP, CNRS, Sorbonne Université, F-75005 Paris, France

Camila Bussola Tovani − Collège de France, Laboratoire Chimie de la Matière Condensée de Paris, LCMCP, CNRS, Sorbonne Université, F-75005 Paris, France

Yan Wang − Collège de France, Laboratoire Chimie de la Matière Condensée de Paris, LCMCP, CNRS, Sorbonne Université, F-75005 Paris, France

Fabrice Soncin − CNRS, Institut Pasteur de Lille, UMR 8161 - M3T - Mechanisms of Tumorigenesis and Target Therapies, Université de Lille, F-59000 Lille, France

Sidney Delgado − MNHN, CNRS, EPHE, Institut Systématique Évolution Biodiversité, ISYEB, Equipe Homologies, Sorbonne Université, 75005 Paris, France

Thierry Azaïs − Collège de France, Laboratoire Chimie de la Matière Condensée de Paris, LCMCP, CNRS, Sorbonne Université, F-75005 Paris, France; ⓞ orcid.org/0000-0002-9031-872X

Capucine Sassoye − Collège de France, Laboratoire Chimie de la Matière Condensée de Paris, LCMCP, CNRS, Sorbonne Université, F-75005 Paris, France; ⓞ orcid.org/0000-0003-2790-888X

Marie-Madeleine Giraud-Guille − Collège de France, Laboratoire Chimie de la Matière Condensée de Paris, LCMCP, CNRS, Sorbonne Université, F-75005 Paris, France

Jean-Yves Sire − MNHN, CNRS, EPHE, Institut Systématique Évolution Biodiversité, ISYEB, Equipe Homologies, Sorbonne Université, 75005 Paris, France

Complete contact information is available at:
https://pubs.acs.org/10.1021/acs.biomac.1c00206

Notes

The authors declare no competing financial interest.

■ ACKNOWLEDGMENTS

■ REFERENCES

(1) Jackson, S. F. The Fine Structure of Developing Bone in the Embryonic Fowl. *Proc. R. Soc. London, Ser. B* **1957**, *146* (923), 270−280.

(2) Weiner, S.; Traub, W. Organization of Hydroxyapatite Crystals within Collagen Fibrils. *FEBS Lett.* **1986**, *206* (2), 262−266.

(3) Xu, Y. F.; Nudelman, F.; Eren, E. D.; Wirix, M. J. M.; Cantaert, B.; Nijhuis, W. H.; Hermida-Merino, D.; Portale, G.; Bomans, P. H. H.; Ottmann, C.; et al. Intermolecular Channels Direct Crystal Orientation in Mineralized Collagen. *Nat. Commun.* **2020**, *11* (1), 5068.

(4) Landis, W. J.; Hodgens, K. J.; Song, M. J.; Arena, J.; Kiyonaga, S.; Marko, M.; Owen, C.; McEwen, B. F. Mineralization of Collagen May Occur on Fibril Surfaces: Evidence from Conventional and High-Voltage Electron Microscopy and Three-Dimensional Imaging. *J. Struct. Biol.* **1996**, *117* (1), 24−35.

(5) Giraud-Guille, M.-M. Plywood Structures in Nature. *Curr. Opin. Solid State Mater. Sci.* **1998**, *3* (3), 221−227.

(6) Garnero, P. The Role of Collagen Organization on the Properties of Bone. *Calcif. Tissue Int.* **2015**, *97* (3), 229−240.

(7) Nassif, N.; Gobeaux, F.; Seto, J.; Belamie, E.; Davidson, P.; Panine, P.; Mosser, G.; Fratzl, P.; Giraud Guille, M. M. Self-Assembled Collagen-Apatite Matrix with Bone-like Hierarchy. *Chem. Mater.* **2010**, *22* (11), 3307−3309.

(8) Wang, Y.; Azaïs, T.; Robin, M.; Vallée, A.; Catania, C.; Legriel, P.; Pehau-Arnaudet, G.; Babonneau, F.; Giraud-Guille, M. M.; Nassif, N. The Predominant Role of Collagen in the Nucleation, Growth, Structure and Orientation of Bone Apatite. *Nat. Mater.* **2012**, *11* (8), 724−733.

(9) Hunter, G. K.; Goldberg, H. A. Nucleation of Hydroxyapatite by Bone Sialoprotein. *Proc. Natl. Acad. Sci. U. S. A.* **1993**, *90* (18), 8562−8565.

(10) Frenkel-Mullerad, H.; Avnir, D. Sol-Gel Materials as Efficient Enzyme Protectors: Preserving the Activity of Phosphatases under Extreme PH Conditions. *J. Am. Chem. Soc.* **2005**, *127* (22), 8077−8081.

(11) Weiner, S.; Wagner, H. D. The Material Bone: Structure-Mechanical Function Relations. *Annu. Rev. Mater. Sci.* **1998**, *28* (1), 271−298.

(12) Reznikov, N.; Shahar, R.; Weiner, S. Bone Hierarchical Structure in Three Dimensions. *Acta Biomater.* **2014**, *10* (9), 3815−3826.

(13) Kokubo, T.; Takadama, H. How Useful Is SBF in Predicting in Vivo Bone Bioactivity? *Biomaterials* **2006**, *27* (15), 2907−2915.

(14) He, G.; Dahl, T.; Veis, A.; George, A. Nucleation of Apatite Crystals in Vitro by Self-Assembled Dentin Matrix Protein 1. *Nat. Mater.* **2003**, *2* (8), 552−558.

(15) Tartaix, P. H.; Doulaverakis, M.; George, A.; Fisher, L. W.; Butler, W. T.; Qin, C.; Salih, E.; Tan, M.; Fujimoto, Y.; Spevak, L.; et al. In Vitro Effects of Dentin Matrix Protein-1 on Hydroxyapatite Formation Provide Insights into in Vivo Functions. *J. Biol. Chem.* **2004**, *279* (18), 18115−18120.

(16) George, A.; Sabsay, B.; Simonian, P. A. L.; Veis, A. Characterization of a Novel Dentin Matrix Acidic Phosphoprotein. Implications for Induction of Biomineralization. *J. Biol. Chem.* **1993**, *268* (17), 12624−12630.

(17) Macdougall, M.; Gu, T. T.; Luan, X.; Simmons, D.; Chen, J. Identification of a Novel Isoform of Mouse Dentin Matrix Protein 1: Spatial Expression in Mineralized Tissues. *J. Bone Miner. Res.* **1998**, *13* (3), 422−431.

(18) Feng, J. Q.; Ward, L. M.; Liu, S.; Lu, Y.; Xie, Y.; Yuan, B.; Yu, X.; Rauch, F.; Davis, S. I.; Zhang, S.; et al. Loss of DMP1 Causes Rickets and Osteomalacia and Identifies a Role for Osteocytes in Mineral Metabolism. *Nat. Genet.* **2006**, *38* (11), 1310−1315.

(19) Lorenz-Depiereux, B.; Bastepe, M.; Benet-Pagès, A.; Amyere, M.; Wagenstaller, J.; Müller-Barth, U.; Badenhoop, K.; Kaiser, S. M.; Rittmaster, R. S.; Shlossberg, A. H.; et al. DMP1Mutations in Autosomal Recessive Hypophosphatemia Implicate a Bone Matrix Protein in the Regulation of Phosphate Homeostasis. *Nat. Genet.* **2006**, *38* (11), 1248−1250.

(20) Mäkitie, O.; Pereira, R. C.; Kaitila, I.; Turan, S.; Bastepe, M.; Laine, T.; Kröger, H.; Cole, W. G.; Jüppner, H. Long-Term Clinical Outcome and Carrier Phenotype in Autosomal Recessive Hypo-phosphatemia Caused by a Novel DMP1Mutation. *J. Bone Miner. Res.* **2010**, *25* (10), 2165−2174.

(21) Turan, S.; Aydin, C.; Bereket, A.; Akcay, T.; Güran, T.; Yaralioglu, B. A.; Bastepe, M.; Jüppner, H. Identification of a Novel Dentin Matrix Protein-1 (DMP-1) Mutation and Dental Anomalies in a Kindred with Autosomal Recessive Hypophosphatemia. *Bone* **2010**, *46* (2), 402−409.

(22) Ye, L.; Mishina, Y.; Chen, D.; Huang, H.; Dallas, S. L.; Dallas, M. R.; Sivakumar, P.; Kunieda, T.; Tsutsui, T. W.; Boskey, A.; et al. Dmp1-Deficient Mice Display Severe Defects in Cartilage Formation Responsible for a Chondrodysplasia-like Phenotype. *J. Biol. Chem.* **2005**, *280* (7), 6197−6203.

(23) Ye, L.; MacDougall, M.; Zhang, S.; Xie, Y.; Zhang, J.; Li, Z.; Lu, Y.; Mishina, Y.; Feng, J. Q. Deletion of Dentin Matrix Protein-1 Leads to a Partial Failure of Maturation of Predentin into Dentin, Hypomineralization, and Expanded Cavities of Pulp and Root Canal during Postnatal Tooth Development. *J. Biol. Chem.* **2004**, *279* (18), 19141−19148.

(24) He, G.; Gajjeraman, S.; Schultz, D.; Cookson, D.; Qin, C.; Butler, W. T.; Hao, J.; George, A. Spatially and Temporally Controlled Biomineralization Is Facilitated by Interaction between Self-Assembled Dentin Matrix Protein 1 and Calcium Phosphate Nuclei in Solution. *Biochemistry* **2005**, *44* (49), 16140−16148.

(25) Tsuji, T.; Onuma, K.; Yamamoto, A.; Iijima, M.; Shiba, K. Direct Transformation from Amorphous to Crystalline Calcium Phosphate Facilitated by Motif-Programmed Artificial Proteins. *Proc. Natl. Acad. Sci. U. S. A.* **2008**, *105* (44), 16866−16870.

(26) He, G.; Dahl, T.; Veis, A.; George, A. Dentin Matrix Protein 1 Initiates Hydroxyapatite Formation in Vitro. *Connect. Tissue Res.* **2003**, *44* (1), 240−245.

(27) Gericke, A.; Qin, C.; Sun, Y.; Redfern, R.; Redfern, D.; Fujimoto, Y.; Taleb, H.; Butler, W. T.; Boskey, A. L. Different Forms of DMP1 Play Distinct Roles in Mineralization. *J. Dent. Res.* **2010**, *89* (4), 355−359.

(28) Huang, J.; Wong, C.; George, A.; Kaplan, D. L. The Effect of Genetically Engineered Spider Silk-Dentin Matrix Protein 1 Chimeric Protein on Hydroxyapatite Nucleation. *Biomaterials* **2007**, *28* (14), 2358−2367.

(29) He, G.; George, A. Dentin Matrix Protein 1 Immobilized on Type I Collagen Fibrils Facilitates Apatite Deposition in Vitro. *J. Biol. Chem.* **2004**, *279* (12), 11649−11656.

(30) Beniash, E.; Deshpande, A. S.; Fang, P. A.; Lieb, N. S.; Zhang, X.; Sfeir, C. S. Possible Role of DMP1 in Dentin Mineralization. *J. Struct. Biol.* **2011**, *174* (1), 100−106.

(31) Silvent, J.; Nassif, N.; Helary, C.; Azaïs, T.; Sire, J. Y.; Giraud-Guille, M. M. Collagen Osteoid-Like Model Allows Kinetic Gene Expression Studies of Non-Collagenous Proteins in Relation with Mineral Development to Understand Bone Biomineralization. *PLoS One* **2013**, *8* (2), e57344.

(32) Retana-Lobo, C.; Guerreiro-Tanomaru, J. M.; Tanomaru-Filho, M.; de Souza, B. D. M.; Reyes-Carmona, J. Non-Collagenous Dentin Protein Binding Sites Control Mineral Formation during the Biomineralisation Process in Radicular Dentin. *Materials* **2020**, *13* (5), 1053.

(33) Gajjeraman, S.; Narayanan, K.; Hao, J.; Qin, C.; George, A. Matrix Macromolecules in Hard Tissues Control the Nucleation and Hierarchical Assembly of Hydroxyapatite. *J. Biol. Chem.* **2007**, *282* (2), 1193−1204.

(34) Bedran-Russo, A. K.; Ravindran, S.; George, A. Imaging Analysis of Early DMP1Mediated Dentine Remineralization. *Arch. Oral Biol.* **2013**, *58* (3), 254−260.

(35) Qin, C.; Brunn, J. C.; Cook, R. G.; Orkiszewski, R. S.; Malone, J. P.; Veis, A.; Butler, W. T. Evidence for the Proteolytic Processing of Dentin Matrix Protein 1: Identification and Characterization of Processed Fragments and Cleavage Sites. *J. Biol. Chem.* **2003**, *278* (36), 34700−34708.

(36) Qin, C.; Huang, B.; Wygant, J. N.; McIntyre, B. W.; McDonald, C. H.; Cook, R. G.; Butler, W. T. A Chondroitin Sulfate Chain Attached to the Bone Dentin Matrix Protein 1 NH2-Terminal Fragment. *J. Biol. Chem.* **2006**, *281* (12), 8034−8040.

(37) Silvent, J.; Sire, J. Y.; Delgado, S. The Dentin Matrix Acidic Phosphoprotein 1 (DMP1) in the Light of Mammalian Evolution. *J. Mol. Evol.* **2013**, *76* (1−2), 59−70.

(38) Lu, Y.; Yuan, B.; Qin, C.; Cao, Z.; Xie, Y.; Dallas, S. L.; McKee, M. D.; Drezner, M. K.; Bonewald, L. F.; Feng, J. Q. The Biological Function of DMP-1 in Osteocyte Maturation Is Mediated by Its 57-KDa c-Terminal Fragment. *J. Bone Miner. Res.* **2011**, *26* (2), 331−340.

(39) Deshpande, A. S.; Fang, P. A.; Zhang, X.; Jayaraman, T.; Sfeir, C.; Beniash, E. Primary Structure and Phosphorylation of Dentin Matrix Protein 1 (DMP1) and Dentin Phosphophoryn (DPP) Uniquely Determine Their Role in Biomineralization. *Biomacromolecules* **2011**, *12* (8), 2933−2945.

(40) Ling, Y.; Rios, H. F.; Myers, E. R.; Lu, Y.; Feng, J. Q.; Boskey, A. L. DMP1 Depletion Decreases Bone Mineralization in Vivo: An FTIR Imaging Analysis. *J. Bone Miner. Res.* **2005**, *20* (12), 2169−2177.

(41) Burgener, B.; Ford, A. R.; Situ, H.; Fayad, M. I.; Hao, J. J.; Wenckus, C. S.; Johnson, B. R.; Begole, E. A.; George, A. Biologic Markers for Odontogenic Periradicular Periodontitis. *J. Endod.* **2010**, *36* (8), 1307−1310.

(42) Sato, S.; Hashimoto, J.; Usami, Y.; Ohyama, K.; Isogai, Y.; Hagiwara, Y.; Maruyama, N.; Komori, T.; Kuroda, T.; Toyosawa, S. Novel Sandwich ELISAs for Rat DMP1: Age-Related Decrease of Circulatory DMP1 Levels in Male Rats. *Bone* **2013**, *57* (2), 429−436.

(43) Bradt, J. H.; Mertig, M.; Teresiak, A.; Pompe, W. Biomimetic Mineralization of Collagen by Combined Fibril Assembly and Calcium Phosphate Formation. *Chem. Mater.* **1999**, *11* (10), 2694−2701.

(44) Olszta, M. J.; Cheng, X.; Jee, S. S.; Kumar, R.; Kim, Y. Y.; Kaufman, M. J.; Douglas, E. P.; Gower, L. B. Bone Structure and Formation: A New Perspective. *Mater. Sci. Eng., R* **2007**, *58* (3−5), 77−116.

(45) Nudelman, F.; Pieterse, K.; George, A.; Bomans, P. H. H.; Friedrich, H.; Brylka, L. J.; Hilbers, P. A. J.; De With, G.; Sommerdijk, N. A. J. M. The Role of Collagen in Bone Apatite Formation in the Presence of Hydroxyapatite Nucleation Inhibitors. *Nat. Mater.* **2010**, *9* (12), 1004−1009.

(46) Bradt, J. H.; Mertig, M.; Teresiak, A.; Pompe, W. Biomimetic Mineralization of Collagen by Combined Fibril Assembly and Calcium Phosphate Formation. *Chem. Mater.* **1999**, *11* (10), 2694−2701.

(47) Gower, L. B. Biomimetic Model Systems for Investigating the Amorphous Precursor Pathway and Its Role in Biomineralization. *Chem. Rev.* **2008**, *108* (11), 4551−4627.

(48) Glimcher, M. J.; Hodge, A. J.; Schmitt, F. O. Macromolecular Aggregation States in Relation to Mineralization: The Collagen-Hydroxyapatite System as Studied in Vitro. *Proc. Natl. Acad. Sci. U. S. A.* **1957**, *43* (10), 860−867.

(49) Lee, D. D.; Glimcher, M. J. Three-Dimensional Spatial Relationship between the Collagen Fibrils and the Inorganic Calcium Phosphate Crystals of Pickerel (Americanus Americanus) and Herring (Clupea Harengus) Bone. *J. Mol. Biol.* **1991**, *217* (3), 487−501.

(50) Brown, W. E.; Eidelman, N.; Tomazic, B. Octacalcium Phosphate as a Precursor in Biomineral Formation. *Adv. Dent. Res.* **1987**, *1* (2), 306−313.

(51) Crane, N. J.; Popescu, V.; Morris, M. D.; Steenhuis, P.; Ignelzi, M. A. Raman Spectroscopic Evidence for Octacalcium Phosphate and Other Transient Mineral Species Deposited during Intramembranous Mineralization. *Bone* **2006**, *39* (3), 434−442.

(52) Gobeaux, F.; Belamie, E.; Mosser, G.; Davidson, P.; Panine, P.; Giraud-Guille, M. M. Cooperative Ordering of Collagen Triple Helices in the Dense State. *Langmuir* **2007**, *23* (11), 6411−6417.

(53) Bergman, I.; Loxley, R. Two Improved and Simplified Methods for the Spectrophotometric Determination of Hydroxyproline. *Anal. Chem.* **1963**, *35* (12), 1961−1965.

(54) Rhee, S. H.; Tanaka, J. Hydroxyapatite Formation on Cellulose Cloth Induced by Citric Acid. *J. Mater. Sci.: Mater. Med.* **2000**, *11* (7), 449−452.

(55) Marelli, B.; Ghezzi, C. E.; Barralet, J. E.; Nazhat, S. N. Collagen Gel Fibrillar Density Dictates the Extent of Mineralization in Vitro. *Soft Matter* **2011**, *7* (21), 9898−9907.

(56) Knight, D. P.; Nash, L.; Hu, X. W.; Haffegee, J.; Ho, M.-W. In Vitro Formation by Reverse Dialysis of Collagen Gels Containing Highly Oriented Arrays of Fibrils. *J. Biomed. Mater. Res.* **1998**, *41* (2), 185−191.

(57) Kokubo, T.; Takadama, H. How Useful Is SBF in Predicting in Vivo Bone Bioactivity? *Biomaterials* **2006**, *27* (15), 2907−2915.

(58) Bonewald, L. F.; Harris, S. E.; Rosser, J.; Dallas, M. R.; Dallas, S. L.; Camacho, N. P.; Boyan, B.; Boskey, A. Von Kossa Staining Alone Is Not Sufficient to Confirm That Mineralization in Vitro Represents Bone Formation. *Calcif. Tissue Int.* **2003**, *72* (5), 537−547.

(59) Nassif, N.; Martineau, F.; Syzgantseva, O.; Gobeaux, F.; Willinger, M.; Coradin, T.; Cassaignon, S.; Azaïs, T.; Giraud-Guille, M. M. In Vivo Inspired Conditions to Synthesize Biomimetic Hydroxyapatite. *Chem. Mater.* **2010**, *22* (12), 3653−3663.

(60) Dorozhkin, S. V.; Epple, M. Biological and Medical Significance of Calcium Phosphates. *Angew. Chem., Int. Ed.* **2002**, *41* (17), 3130−3146.

(61) Landis, W. J.; Glimcher, M. J. Electron Diffraction and Electron Probe Microanalysis of the Mineral Phase of Bone Tissue Prepared by Anhydrous Techniques. *J. Ultrastruct. Res.* **1978**, *63* (2), 188−223.

(62) Matsumoto, M.; Miyake, T.; Noshi, H.; Kambara, M.; Konishi, K. Zeta Potential Studies on the Adsorption of Proteins on a Synthetic Hydroxyapatite. *Colloids Surf.* **1989**, *40*, 77−84.

(63) Niu, L. N.; Jee, S. E.; Jiao, K.; Tonggu, L.; Li, M.; Wang, L.; Yang, Y. D.; Bian, J. H.; Breschi, L.; Jang, S. S.; et al. Collagen Intrafibrillar Mineralization as a Result of the Balance between Osmotic Equilibrium and Electroneutrality. *Nat. Mater.* **2017**, *16* (3), 370−378.

(64) Lucent, D.; Vishal, V.; Pande, V. S. Protein Folding under Confinement: A Role for Solvent. *Proc. Natl. Acad. Sci. U. S. A.* **2007**, *104* (25), 10430−10434.

(65) Sarem, M.; Lüdeke, S.; Thomann, R.; Salavei, P.; Zou, Z.; Habraken, W.; Masic, A.; Shastri, V. P. Disordered Conformation with Low Pii Helix in Phosphoproteins Orchestrates Biomimetic Apatite Formation. *Adv. Mater.* **2017**, *29* (35), 1701629.

(66) Wang, Y.; Von Euw, S.; Laurent, G.; Crevant, C.; Bonhomme-Coury, L.; Giraud-Guille, M. M.; Babonneau, F.; Nassif, N.; Azaïs, T. Impact of Collagen Confinement vs. Ionic Substitutions on the Local Disorder in Bone and Biomimetic Apatites. *Mater. Horiz.* **2014**, *1* (2), 224−231.

(67) Jee, S. S.; Culver, L.; Li, Y.; Douglas, E. P.; Gower, L. B. Biomimetic Mineralization of Collagen via an Enzyme-Aided PILP Process. *J. Cryst. Growth* **2010**, *312* (8), 1249−1256.

(68) Thula, T. T.; Rodriguez, D. E.; Lee, M. H.; Pendi, L.; Podschun, J.; Gower, L. B. In Vitro Mineralization of Dense Collagen Substrates: A Biomimetic Approach toward the Development of Bone-Graft Materials. *Acta Biomater.* **2011**, *7* (8), 3158−3169.

(69) Chen, L.; Jacquet, R.; Lowder, E.; Landis, W. J. Refinement of Collagen-Mineral Interaction: A Possible Role for Osteocalcin in Apatite Crystal Nucleation, Growth and Development. *Bone* **2015**, *71*, 7−16.

(70) Chow, W. Y.; Rajan, R.; Muller, K. H.; Reid, D. G.; Skepper, J. N.; Wong, W. C.; Brooks, R. A.; Green, M.; Bihan, D.; Farndale, R. W.; et al. NMR Spectroscopy of Native and in Vitro Tissues Implicates PolyADP Ribose in Biomineralization. *Science* **2014**, *344* (6185), 742−746.

(71) Gautieri, A.; Pate, M. I.; Vesentini, S.; Redaelli, A.; Buehler, M. J. Hydration and Distance Dependence of Intermolecular Shearing between Collagen Molecules in a Model Microfibril. *J. Biomech.* **2012**, *45* (12), 2079−2083.

(72) Fratzl, P.; Fratzl-Zelman, N.; Klaushofer, K. Collagen Packing and Mineralization. An x-Ray Scattering Investigation of Turkey Leg Tendon. *Biophys. J.* **1993**, *64* (1), 260−266.

(73) Glimcher, M. J.; Krane, S. M. The Incorporation of Radioactive Inorganic Orthophosphate as Organic Phosphate by Collagen Fibrils in Vitro. *Biochemistry* **1964**, *3* (2), 195−202.

(74) Kim, D.; Lee, B.; Thomopoulos, S.; Jun, Y. S. The Role of Confined Collagen Geometry in Decreasing Nucleation Energy Barriers to Intrafibrillar Mineralization. *Nat. Commun.* **2018**, *9* (1), 962.

(75) Akiva, A.; Kerschnitzki, M.; Pinkas, I.; Wagermaier, W.; Yaniv, K.; Fratzl, P.; Addadi, L.; Weiner, S. Mineral Formation in the Larval Zebrafish Tail Bone Occurs via an Acidic Disordered Calcium Phosphate Phase. *J. Am. Chem. Soc.* **2016**, *138* (43), 14481−14487.

(76) Mahamid, J.; Sharir, A.; Addadi, L.; Weiner, S. Amorphous Calcium Phosphate Is a Major Component of the Forming Fin Bones of Zebrafish: Indications for an Amorphous Precursor Phase. *Proc. Natl. Acad. Sci. U. S. A.* **2008**, *105* (35), 12748−12753.

(77) Von Euw, S.; Wang, Y.; Laurent, G.; Drouet, C.; Babonneau, F.; Nassif, N.; Azaïs, T. Bone Mineral: New Insights into Its Chemical Composition. *Sci. Rep.* **2019**, *9* (1), 8456.

(78) Cho, G.; Wu, Y.; Ackerman, J. L. Detection of Hydroxyl Ions in Bone Mineral by Solid-State NMR Spectroscopy. *Science* **2003**, *300* (5622), 1123−1127.

(79) Glimcher, M. J. Bone: Nature of the Calcium Phosphate Crystals and Cellular, Structural, and Physical Chemical Mechanisms in Their Formation. In *Medical Mineralogy and Geochemistry*; Sahai, N., Schoonen, M. A. A., Eds.; De Gruyter: Berlin, Germany, 2006; Vol. 64, pp 223−282.

(80) Engler, A. J.; Sen, S.; Sweeney, H. L.; Discher, D. E. Matrix Elasticity Directs Stem Cell Lineage Specification. *Cell* **2006**, *126* (4), 677−689.